First publ. in: Journal of Vacuum Science and Technology / A, Vacuum, Surfaces, and Films, Vol. 16 (1998), 3, pp. 1239-1243

Submicron contacts for electrical characterization of semiconducting WS_2 thin films

C. Ballif,[a] M. Regula, and F. Lévy
Institute of Applied Physics, Ecole Polytechnique Fédérale de Lausanne, 1015 Lausanne, Switzerland

F. Burmeister, C. Schäfle, Th. Matthes, and P. Leiderer
Universität Konstanz, Fakultät für Physik, 78434 Konstanz, Germany

Ph. Niedermann
Centre Suisse d'Electronique et de Microtechnique SA, 2007 Neuchâtel, Switzerland

W. Gutmannsbauer and R. Bucher
Paul Bucher Company, 4051 Basel, Switzerland

(Received 22 September 1997; accepted 24 November 1997)

We report a new method to characterize the local electronic properties of polycrystalline semiconducting thin films. A lattice of triangular gold electrodes, with a typical area of 0.2 μm^2, is evaporated on a p-type WS_2 film. With the help of a conductive atomic force microscope, the current–voltage characteristics of the contacts established between the gold electrodes and the WS_2 film are measured. A linear dependence of the current versus voltage is obtained on gold triangles in contact with grain edges. This indicates a high level of doping or degeneracy of the semiconductor at the grain edges. The electrodes deposited on flat WS_2 crystallites form rectifying diodes with the underlying grains. Barrier heights of 0.56–0.74 eV and diode ideality factors between 1.15 and 2 are determined. Under illumination, open-circuit voltages up to 500 mV can be measured on some contacts. A short response time of the photocurrent is observed (<0.1 ms) when the diodes are reversed biased, which is related to intrinsic properties of the crystallites. When the diodes are forward biased a longer response time is measured (>100 ms), linked to trapping effects at grain boundaries.

I. INTRODUCTION

Polycrystalline films of semiconductors are important for microelectronics, gas sensors and solar cells. The emergence of the scanning probe techniques like scanning tunnelling microscopy (STM) or atomic force microscopy (AFM) makes it possible to access directly the local properties of thin films. This can be of crucial importance in the case of multiphase, inhomogeneous materials, percolative systems or when the properties at grain boundaries are different from the bulk. In this article, we present a simple method that yields quantitative information on the properties of crystallites and grain boundaries of WS_2 thin films. Such films have been intensively studied in the last years, due to their potential in photovoltaic application.[1–10]

An array of metallic electrodes, smaller than the typical lateral crystallite size, is deposited on a thin film. It is expected that some electrodes are deposited on crystallites, touching no grain boundaries, while others are in contact with steps or grain edges. Using an atomic force microscope with a conductive tip, the properties of each contact established between the metal electrodes and the semiconductor film are investigated.

Compared to STM or AFM current–voltage ($I-V$) spectroscopy directly on semiconductor surfaces, the method presents several advantages. In the case of STM, severe tip damage can occur if insulating phases, holes in films deposited on insulating substrate, or grains with different doping (changing from p to n) are present. In the case of both STM and AFM, it is not easy to have a stable signal between a metallic tip and a semiconductor due to tip contamination or electrical noise due to the low current flowing, except in very clean conditions. Finally, the usual lack of information on the tip–sample geometry and interaction makes a quantitative interpretation of the results difficult.

In the technique proposed here, the contact AFM mode is controlled independently of the current flowing between the tip and the sample, preventing any damaging to the tip. The contact between the conductive AFM tip and the small electrodes is ohmic, and contributes a series resistance that can be determined directly. The studied metal/semiconductor interface has a precise geometry, therefore allowing quantitative measurements.

If the grain size of the polycrystalline films is in the μm range, the contacts to be deposited must have a typical size of 0.1–1 μm. A simple process to produce an array of contacts on any surface has been developed recently.[11] The process consists of metal evaporation through a versatile lithographic mask, formed by hexagonally closed packed monolayers of colloidal latex spheres. The direct preparation of the colloid monolayers on the film, which is the usual technique for the preparation of structures on glass or Si substrates, is not desirable since solvents or contaminants on the semiconductor surface should be avoided. It is further-

[a]Author to whom correspondence should be addressed; electronic mail: Ballif@ipasg.epfl.ch

1239

more difficult to achieve due to film roughness and the hydrophobic properties of WS_2.

Suitable conductive and wear resistant AFM tips are obtained by chemical vapor deposition (CVD) of boron-doped diamond on commercial Si tips.[12] Such tips resist intensive scanning, and an ohmic contact is obtained between the tip and gold surface.

This method, applied to semiconducting tungsten sulphide thin films, gives new insight into the properties of the films: it shows that photosensitive solid-state metal–semiconductor junctions can be established on the WS_2 film crystallites, providing that no metal touches the grain boundaries. It also shows that the in-plane transport properties are dominated by grain boundary trapping and scattering, while the intrinsic properties of the crystallites are similar to those of single crystals.

II. EXPERIMENTS

The films are prepared by a sputtering/annealing process.[5,7] A 200 nm amorphous layer of WS_{3-4} is sputter-deposited on a quartz substrate coated with 10 nm of Co. After annealing for 1 h at 950 °C under argon flow, WS_2 films are obtained. The effect of Co is to improve the crystallinity of the films.[7]

The preparation of the lithographic mask is described in detail elsewhere.[11] 3 μm latex spheres form the colloid monolayers which are collected on a nickel transmission electron microscopy grid. The resulting mask is put onto the film before the evaporation of 50 nm gold in a chamber with 10^{-4} Pa base pressure. The grid is removed from the sample with a magnet, leaving the sample with the appropriated lattice of submicron contacts.

A Topometrix Explorer AFM, is operated in air in contact mode, with typical scanning frequency of 0.5–1 Hz. The current is measured with an external high-bandpass ($>10^4$ Hz) Keithley K428 current amplifier. The noise level for the current measurement is below 10 pA. The AFM electronics enable simultaneous acquisition of topography information and tip–sample current, as well as $I-V$ measurements at specific locations on the surface. The preparation of diamond coated conductive AFM tips is described elsewhere.[12] The tips have a radius of about 100 nm and a spring constant of 4 N/m. In order to establish a good electrical contact between the tip and the sample, a load of about 50 nN has to be applied. Under these conditions, the contact resistance between the tip and gold is 50 kΩ. Although a load of 50 nN is relatively high, no damage appears to the films, even after intense scanning. If a high voltage ($V>+1$ V) is applied to the film when working in air, an oxidation reaction can take place between the film and the tip resulting in film damage, as already observed on chalcogenide surfaces.[13]

The geometry of the measurement is described in Fig. 1. The second lateral electrode is prepared with silver paste on the side of the film. This electrode forms an ohmic contact with the film and does not influence the measurements. For measurements under illumination, a green laser beam at 2.33 eV (532 nm), just above the direct band gap of WS_2 at 2 eV, illuminates the sample from the backside through the quartz substrate. The light intensity on the sample is 500 W/m^2. As the AFM height is controlled with a red laser diode (692 nm) at a wavelength different from the green excitation source, scanning feedback is not influenced by the illuminating laser.

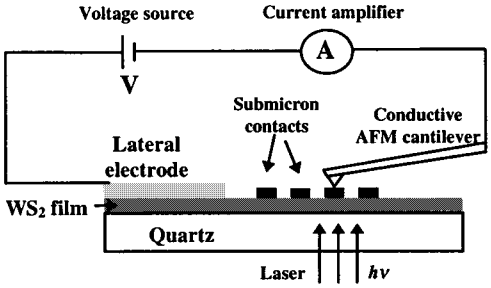

FIG. 1. Experimental setup for the local measurements on the WS_2 thin films.

III. RESULTS AND DISCUSSION

A. Film properties

The WS_2 films crystallize with large, flat crystallites of lateral sizes in the 2–5 μm range. After annealing, no continuous metallic film remains at the substrate–film interface. Most of the cobalt segregates and form large (1 μm) metallic CoS_x droplets.[7] In transmission electron microscopy, no Co is detected in the WS_2 crystallites [energy dispersive spectra (EDS), electron energy-loss spectra (EELS) analysis]. The cobalt influences the in-plane electrical properties of the film mainly through its action on the grain boundaries, like introduction of deep traps or of interface states at the grain edges. From Hall and resistivity measurements, the mobility and carrier concentration are estimated to be in the range of 5–10 cm^2/V s and 10^{17} cm^{-3} at room temperature. Both mobility and carrier concentration appear thermally activated, with activation energies of about 80 meV and 60 meV, respectively. The optical absorption coefficient is similar to those of single crystals, showing an indirect band gap at 1.3 eV, and the first exciton peak associated with the lowest direct transition at 1.95 eV. In photoconductivity experiments, a long lifetime of the carrier is observed, of the order of 0.1 s.

B. Deposition of microcontacts and current mapping

Figures 2(a) and 2(b) show AFM topography images of a WS_2 film with evaporated gold electrodes. The lateral size of the triangular contacts is approximately 0.7 μm, yielding a surface of 0.2 μm^2 for a single contact. Due to imperfections of the mask (nonuniformity in the size of the latex spheres, for instance) larger contacts formed by connected triangles are also observed.

Figure 3 shows the mapping of the current during scanning in four different conditions acquired on the topography of Fig. 2(b). The gray scale for the current is the same for the four images, ranging from +1 nA (white) to −1 nA (black). In Figs. 3(a) and 3(b), a negative voltage is applied to the film (−100 mV), which produces an inverse polarization

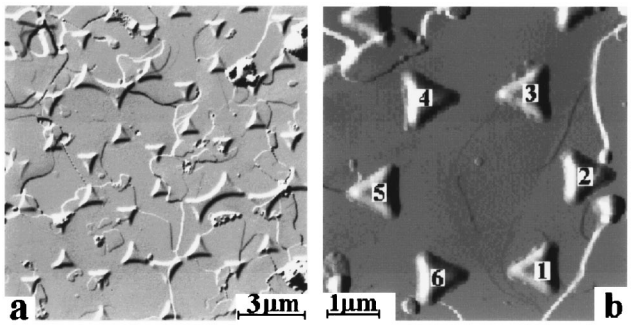

FIG. 2. AFM topography images showing triangular gold electrodes deposited on a WS_2 thin film. The electrodes have been deposited by evaporation through a mask formed by an hexagonal lattice of 3 μm latex spheres. The large round grains are CoS_x phases. The current flowing through contacts 1–6 of (b) is shown in Fig. 3.

in a p-type semiconductor/metal junction. In Fig. 3(a), the laser is off, and no current flows through contacts 1,3,4 and 5 [numbers refer to Fig. 2(b) contacts]. Under illumination [Fig. 3(b)], a reverse current flows and these contacts appear black. When a small positive voltage is applied to the film [+20 mV, Fig. 3(c), laser off], a positive current flows through contact 2 and a weak current flows through contact 6. If the laser is switched on [Fig. 3(d)], a positive current still goes through contact 2, but contacts 1,3,4, and 6 appear black, indicating that a negative current flows under positive bias. These contacts are working in solar cell mode, with open-circuit voltage (V_{oc}) higher than 20 mV. Contact 5 has disappeared from Fig. 3(d) because its V_{oc} is approximately 20 mV. In every case, a high current ($|I|>>1$ nA) flows through contact 2.

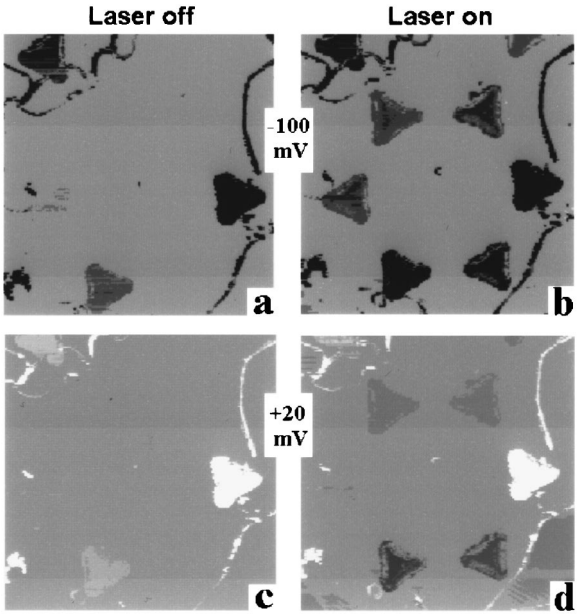

FIG. 3. Current images acquired in four different conditions, with the substrate polarized negatively or positively (−100 mV and +20 mV) and with the laser on or off. (a) V=−100 mV, laser off. (b) V=−100 mV, laser on. (c) V=+20 mV, laser off. (d) V=+20 mV, laser on. The current scale covers a range of 2 nA (white=1 nA, black=−1 nA, grey=0 nA).

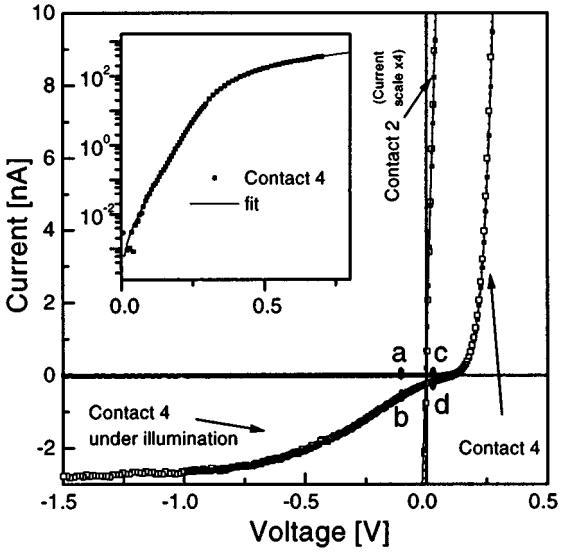

FIG. 4. $I-V$ characteristics on contacts 2 and 4 of Fig. 2(b), in darkness (black symbols) and under illumination (hollow symbols). The insert shows the logarithmic dependence of the current through diode 4 as a function of the applied voltage, and a fit of the diode dark $I-V$ characteristic.

All the results are confirmed by the $I-V$ characteristics with and without illumination on the different contacts. Figure 4 shows $I-V$ curves obtained on contacts 4 and 2. Points a,b,c, and d in Fig. 4 correspond to the values obtained when mapping the current on contact 4. Under illumination, a V_{oc} of 110 mV and a short-circuit current $I_{sc}=0.3$ nA are measured. The insert shows a logarithmic plot of the dark current on contact 4 and a simulation using the equation $I_{dark}=I_s\{\exp[q(V-R_sI_{dark})/nkT]-1\}$,[14] where R_s is a series resistance, I_s the saturation current, and n the diode ideality factor. The dark $I-V$ curve is perfectly reproduced with the fitting parameters n=1.15, $R_s=1.1$ MΩ and $I_s=1.89\times10^{-3}$ nA. The current through contact 2 follows a linear law with a resistance of 1 MΩ. It is approximately the same as the series resistance for diode 4. Diode 4 has the highest measured open-circuit voltage of the five diodes on images 3, but contacts 1 and 6 have higher short-circuit current, which explains their darker appearance in Fig. 3(d).

In general the following observations are made:

(i) All contacts which are on flat areas and touch no grain edges show rectifying behavior, with no current flowing up to −3 V. Barrier heights estimated from the saturation current density J_s range from 0.54 to 0.72 V, for J_s varying between 10^{-2} and 10^{-5} A/cm^2. Under illumination, open-circuit voltages up to 500 mV and short-circuit currents of up to 1.6 nA are observed. The diode series resistance is associated with the resistance of the path of the current from the crystallite to the silver paste electrode. It is typically in the MΩ range, which is an order of magnitude larger than both the AFM tip–gold resistance and the spreading resistance associated with the contact (R∼1Ω cm/1 μm=10 kΩ[14]).

(ii) The AFM current images show that a high current flows at low voltage between the tip and the grain edges. This indicates that the semiconductor is degenerate at grain

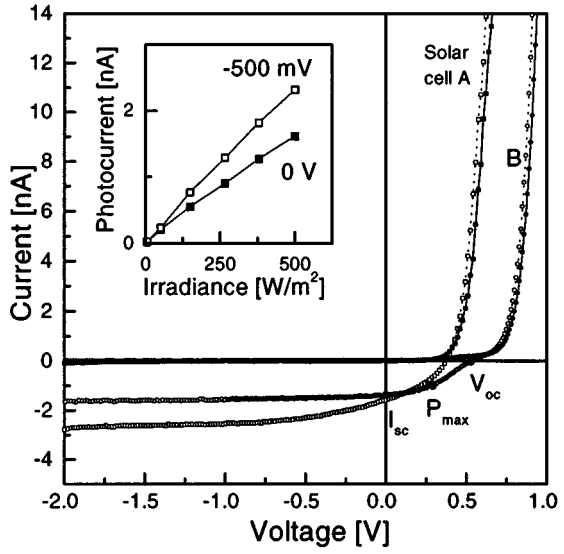

FIG. 5. $I-V$ characteristics on two gold/WS_2 micro-solar cells A and B, in darkness (black symbols) and under illumination (hollow symbols). The dependence of the photocurrent vs light intensity for contact A at 0 and -500 mV is given in inset.

boundaries. Contacts touching grain edges show linear or degenerated diode $I-V$ characteristics. The typical resistance associated with such contacts is again in the MΩ range and has the same origin as the series resistance measured for the diodes. In fact, all intermediate cases to (i) and (ii), are observed from the perfect diode to the simple resistance, passing through diodes with low shunt resistance and high saturation current.

(iii) Under illumination, a photocurrent flows sometimes between the tip and the semiconductor surface [see Fig. 3(d), on the crystallite's lower right side]. This current is however very unstable and very sensitive to tip contamination. In principle, when working in high vacuum condition, a good quality mapping of the photo-induced current between the tip and the WS_2 crystallites should be possible. Similar experiments have been realized using high-vacuum STM on WS_2 surfaces.[15]

C. Micro-solar cells

Figure 5 shows $I-V$ characteristics for two contacts, A and B, in darkness and under illumination. Contact A has a V_{oc} of 360 mV, an I_{sc} of 1.6 nA, and a fill factor of 38%. Contact B has a V_{oc} of 520 mV and an I_{sc} of 1.4 nA. The output power is maximum at 0.3 V, with $P_{max}=0.3$ nW, yielding a 41% fill factor. For most micro-solar cells, the photocurrent is voltage dependent and there is a crossing of the dark and light $I-V$ curves. This indicates that the superposition principle $I=I_{dark}+I_{light}$ is not valid. However, in short-circuit condition and under reverse bias, I_{light} increases linearly with the light intensity as shown in the Fig. 5 inset. For most diodes, a photoinduced current of about 3 nA is reached under a reverse bias of -2 V. In these conditions, the light has to be collected on an area A of 22 μm^2 to produce such a current (with irradiance P=500 W/m^2, fraction of absorbed light at 532 nm f=55%). This is approximately the surface of the crystallites on which the micro-solar cells are formed. With such an area for the collection of the photo-generated carriers, the efficiency of the solar cell B at 532 nm can be estimated: the absorbed incident power is $P\times f\times A=500\times 0.55\times 22\times 10^{-12}=6.05$ nW, when the device maximum output power is 0.3 nW. This yields an efficiency of 5% at 532 nm.

The quantities measured on the micro-solar cells, like V_{oc} or the fill factor, are comparable to what is obtained for solid state devices based on layered chalcogenides single crystals.[1] The values of the short-circuit current density, J_{sc}, are also reasonable if we consider collections of carriers limited laterally by the grain boundaries (near 10 mA/cm^2 under the preceding assumptions). In dark condition, the good diode ideality factors (1.15–2) and high rectifying ratio (current below 10 pA at -1 V) are explained by the quasi-ideal junction realised by the micro-contacts, whereas in macroscopic junctions realized with WSe_2 single crystals[16] or WS_2 films,[3,8,9] surface defects or grain boundaries induce shunt resistance and nonideal dark $I-V$ characteristics. Now, the shape of the $I-V$ curves under illumination is briefly discussed.

When the diode is forward biased (V>0.6 V typically), a decrease of the series resistance due to in-plane photoconductivity is the dominant effect. At lower voltage, photoconduction through the film is not sufficient to explain the intersection of the dark and illuminated curve in the first quadrant. This effect has, however, already been observed for solar cells based on single crystals of the layered compound ReS_2[17] and on WS_2 solar cells.[3] Nonideal behavior under illumination is also observed for WSe_2 single crystal based solar cell,[18] where it is ascribed to interface states. The shapes of light curves for contact B [Fig. 5] and contact 4 of Fig. 4, might partly be explained by such interface recombination.[18] In our case, due to the thinness of the film ($\sim$150 nm), the width variation of the depletion region with the applied voltage is also an important factor. For a band bending of 1 eV, the depth of the depletion zone is approximately 100 nm (with $p=10^{17}/cm^3$ and $\varepsilon_s/\varepsilon_0=10$). Under reverse bias, the depletion zone must extend laterally into the crystallites. If there is competition between recombination at grain boundaries and collection of the carriers in the space charged region, an extended depletion region enables a larger collection of carriers by the junction. In the extreme case of thin crystallite or lower doping of the grain, the depletion region can reach the grain boundaries, and saturation of the photo-induced current occurs. A saturation of the photocurrent under reverse bias is observed for most of the micro-solar cells. Close to the studied electrodes, the current collection and distribution in the film can also be modified by the presence of other neighboring gold contacts, which induce a band bending even if they are not contacted by the AFM tip. Under illumination, the gold electrodes which are not contacted by the AFM tip will act as recombination centers for the excited carriers, therefore lowering I_{sc} and V_{oc} of the measured electrode.

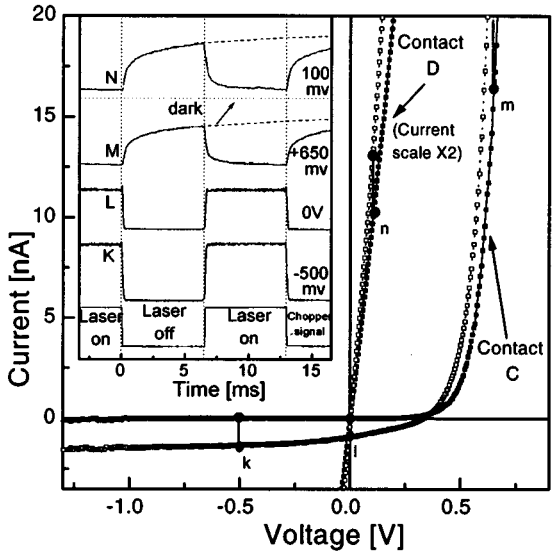

FIG. 6. $I-V$ characteristics in darkness (black symbols) and under illumination (hollow symbols) obtained on two micro-contacts C and D. The insert shows the time dependence of the photocurrent. Curves K, L, M in the inset have been acquired on contact C, at polarisations of -500, 0, and 650 mV, respectively. Curve N is taken on contact D at 100 mV. The photocurrent scale is the same for curves K and L. The curves N and M have amplitudes in the range of 2–5 nA. They have been rescaled to show their similar time dependence. It takes a few seconds for these signals to reach the dark condition equilibrium (dotted line above signal M) when the light is switched off.

D. Transition from local to global properties

The time dependent response to excitation processes are studied on two contacts, C and D, whose characteristics in darkness and under illumination are plotted in Fig. 6. Diode C shows a V_{oc} of 330 mV and a short-circuit current of 0.92 nA. Contact D is noninjecting and has a quasilinear $I-V$ characteristic. On contact C, the voltage is set at three different values: -500, 0, and $+650$ mV. For each value the current response to light chopped at 77 Hz is shown in the Fig. 6 inset. At -500 mV (curve K) and in short-circuit condition (0 V, curve L) the response time is typically shorter than 10^{-4} s. This time is close to the bandpass limit of the current amplifier. The amplitudes of the photocurrent are 1.3 nA at -500 mV and 0.92 nA at 0 V. These values are the same as the ones determined by measuring the current at point k and l on the light $I-V$ curve. When the diode is polarized positively ($+650$ mV), illumination induces an increase of the flowing current, explaining the reversal of the curve M signal. A fast decay (1 ms) is followed by longer lifetimes reaching 100 ms. After switching off the illumination, it takes a few seconds to reach stable dark conditions (dotted line above curve M). These long response times cannot be explained by the diode capacitance under forward bias, which yield an RC time constant shorter than 10^{-6} s. In fact, curve N obtained on the noninjecting contact D polarized with ± 100 mV shows similar behaviour. It has been rescaled to have the same amplitude as curve M, and shows an identical time dependence. Signals M and N are related to the series resistance and to the photoconduction processes. They are similar to those obtained in macroscopic photoconductivity experiments. The long response times are associated with the trapping and release of carriers at grain boundaries. Barriers at grain boundaries control the conductivity through the films and provide an explanation[19] for a thermally activated mobility.

IV. CONCLUSIONS

A simple method for the determination of the electronic properties of semiconducting thin films has been presented. With a conductive AFM scanning a lattice of gold electrodes deposited on a WS_2 thin film, the properties of the film crystallites and grain boundaries have been studied. Grain boundaries are degenerate and degrade the properties of diodes that touch them. They also control the transport properties through the film. When a contact is deposited on a single crystallite, it forms a junction with the semiconductor and acts as a solar cell under illumination.

ACKNOWLEDGMENTS

The authors acknowledge Dr. Ph. Schmid for helpful discussion and B. Gilbert for careful manuscript reading. The project is financially supported by the Fond National Suisse de la Recherche Scientifique and by the Office Fédéral de l'Education et de la Science.

[1] E. Bucher, in *Photoelectrochemistry and Photovoltaics of Layered Semiconductors*, edited by A. Aruchamy (Kluwer, Dordrecht, 1992), pp. 1–81.
[2] M. Genut, L. Margulis, G. Hodes, and R. Tenne, Thin Solid Films **217**, 91 (1992).
[3] A. Jäger-Waldau, M. Ch. Lux-Steiner, E. Bucher, and G. Jäger-Waldau, 23rd IEEE PVSC, Louisville, KY, 10–14 May 1993, p. 597.
[4] A. Ennaoui, S. Fiechter, K. Ellmer, R. Scheer, and K. Diesner, Thin Solid Films **261**, 124 (1995).
[5] C. Ballif, M. Regula, P. E. Schmid, M. Remškar, R. Sanjinés, and F. Lévy, Appl. Phys. A: Solids Surf. **62**, 543 (1996).
[6] T. Tsirlina, S. Cohen, H. Cohen, L. Saphir, M. Peisach, R. Tenne, A. Matthäus, S. Tiefenbacher, W. Jaegermann, E. A. Ponomarev, and C. Lévy-Clément, Sol. Energy Mater. Sol. Cells **44**, 457 (1996).
[7] M. Regula, C. Ballif, M. Remškar, and F. Lévy, J. Vac. Sci. Technol. A **15**, 2323 (1997).
[8] A. Matthäus, A. Ennaoui, S. Fiechter, S. Tiefenbacher, T. Kieswetter, K. Diesner, T. Tsirlina, and R. Tenne, J. Electrochem. Soc. **144**, 1013 (1997).
[9] D. Tonti, F. Varsano, F. Decker , C. Ballif, M. Regula, and M. Remškar, J. Phys. Chem. B **101**, 2485 (1997).
[10] O. Lignier, G. Couturier, J. Tedd, D. Gonbeau, and J. Salardenne, Thin Solid Films **299**, 45 (1997).
[11] F. Burmeister, C. Schäfle, Th. W. Matthes, M. Böhmisch, J. Boneberg, and P. Leiderer, Langmuir **13**, 2983 (1997).
[12] Ph. Niedermann, W. Hänni, N. Blanc, R. Christoph, and J. Burger, J. Vac. Sci. Technol. A **14**, 1233 (1996).
[13] B. Parkinson, J. Am. Chem. Soc. **112**, 7489 (1990).
[14] S. M. Sze, *Physics of Semiconductor Devices*, (Wiley, New York, 1981).
[15] Ch. Sommerhalter, Th. W. Matthes, J. Boneberg, P. Leiderer and M. Ch. Lux- Steiner, J. Vac. Sci. Technol. B **15**, 1876 (1997).
[16] G. Hodes, E. Watkins, D. Mantell, L. J. Brillson, M. Peisach, and A. Wold, J. Appl. Phys. **71**, 5077 (1992).
[17] K. Friemelt, M. Ch. Lux-Steiner, and E. Bucher, 11th European Photovoltaics Solar Energy Conference, Montreux, 1992, p. 950.
[18] M. Vögt, K. Friemelt, M. Ch. Lux-Steiner, M. Keilm, W. Reetz, and E. Bucher, 10th European Photovoltaics Solar Energy Conference, Lisbon, 1991, p. 601.
[19] J. W. Orton and M. J. Powell, Rep. Prog. Phys. **43**, 81 (1980).